energies

MDPI

Article

Smart Load Management with Energy Storage for Power Quality Enhancement in Wind-Powered Oil and Gas Applications

Erick Alves [1,*,†], Santiago Sanchez [1,†], Danilo Brandao [2,‡] and Elisabetta Tedeschi [1,†]

[1] Department of Electric Power Engineering, Norwegian University of Science and Technology (NTNU), 7034 Trondheim, Norway
[2] Graduate Program in Electrical Engineering, Universidade Federal de Minas Gerais (UFMG), Belo Horizonte 31270-901, Brazil
* Correspondence: erick.f.alves@ntnu.no
† Current address: O.S. Bragstads Plass 2E, 7034 Trondheim, Norway.
‡ Current address: Av. Antônio Carlos, 6627, Campus Pampulha, Belo Horizonte 31270-901, MG, Brazil.

Received: 3 May 2019; Accepted: 17 July 2019; Published: 2 August 2019

Abstract: This paper investigates power quality issues in a wind-powered offshore oil and gas platform operating in island mode. Topics of interest are the negative effects that load and wind power variability have on the electrical system frequency and voltage; and how those influence the gas turbine operation. The authors discuss how smart load management together with energy storage can mitigate those effects, and propose a control algorithm for that. Simulations in MATLAB/Simulink demonstrate that the proposed energy storage controller reduces frequency and voltage variations in a case study. Moreover, the paper presents a methodology to derive a simplified model of the hybrid energy system that reduces simulation time in at least two orders of magnitude. The latter can be a useful tool for optimization algorithms evaluating a huge number of scenarios, especially those dealing with economical dispatch of generators or sizing of energy storage systems.

Keywords: smart grids; hybrid energy systems; energy management; load management; power quality; oil and gas platforms; energy storage

1. Introduction

Offshore oil and gas platforms (OOGPs) are energy-intensive environments, where power demand is typically larger than 30 MW and natural gas is widely used to fuel equipment in the production, gathering and processing of gas and conventional crude oil [1]. Hence, in many countries, they contribute greatly to the emission of greenhouse gases (GHGs). For instance, the petroleum sector is the main contributor to GHG emissions in Norway, making up 27.8% of the total in 2017 [2].

This fact led to an increased interest in wind power integration into OOGPs in parallel to gas turbines (GTs) [3–5], especially where power from shore is not feasible, either technically or economically [6]. Also, the industry has a strong interest in this concept, and pilot installations in the Norwegian Continental Shelf are already planned [7,8].

From an electrical point of view, intermittent wind resources introduce challenges for the stable and efficient operation of this hybrid energy system (HES). In an OOGP, load variations can be sharp and represent a significant part of the total generation capacity. On top of that, stochastic variations are added on the generation side when wind power is integrated. This raises concerns not only about insufficient amount of inertia, but also excessive frequency and voltage variations during operation that might negatively affect the electrical power quality and the GT operation [9,10]. Hence, during the design phase of a wind-powered OOGP, it is important not only to meet the power balance between

generation and loads, but also consider system dynamics that may affect voltage and frequency in the electrical grid.

From this perspective, energy storage is an enabling technology that can provide proper frequency and voltage regulation, and can then increase frequency and voltage stability in such HES [11,12]. The literature provides several approaches to the problem of optimally designing an energy storage system (ESS) for an HES [13–17], the majority based on solving the unit commitment and economic dispatch problems associating a cost function to the ESS.

However, a common simplification when solving the unit commitment problem is assuming steady-state equations to obtain the active power balance in the system. While valid for an HES connected to a strong grid, this assumption becomes questionable in islanded mode operation or when connected to a weak grid. In those conditions, the ESS is expected to contribute to frequency regulation [11,18], and considerable amounts of energy during a short period of time might be used for this purpose [19]. Furthermore, previous works [20–22] demonstrated that control and energy management strategies might affect substantially the ESS sizing in a stand-alone system.

Within this context, the present work investigates power quality issues in an OOGPs operating in islanded mode where the wind turbine is rated at 36% of the GT nominal power. It is an extension of [10], which combines the previously proposed smart load management strategy with an ESS to mitigate the effects of wind variability. For that, the detailed dynamic model presented in this previous work is used as benchmark, extended to include an ESS, and then compared to the proposed simplified dynamic model in Section 4. The main contributions of this work are:

1. a demonstration of the benefits to power quality that a smart load management together with an ESS can provide in a wind-powered OOGP;
2. a control strategy for the ESS that provides inertial and voltage support to the electrical grid during transients and reduces frequency and voltage variations significantly;
3. a simplified dynamic model of the HES that can be used to optimally design an ESS and dispatch available power sources.

From a control and modeling perspective, there are no large differences in the mathematical tools and techniques applied in the energy management system (EMS) of a wind-powered OOGP when compared to a typical onshore system. Hence, the proposed simplified model and energy storage system controller can be generally applied to any hybrid energy system. However, boundary conditions and constraints may differ significantly. For instance, GTs should supply both electrical and heat power in an OOGP and comply with additional technical and environmental limitations. Typically, poor power quality (i.e., excessive frequency and voltage deviations) can negatively influence the performance of the process. Consequently, the problem formulation and objective functions for economical dispatch and energy storage sizing should be affected.

This paper is organized in the following manner: Section 2 introduces the case study and highlights the main additions compared to the previous contribution [10]; Section 3 presents the negative effects that power fluctuations have on the frequency and voltage of the studied HES in a time scale of seconds. It also demonstrates how those can be counteracted by an ESS providing inertial and voltage support; Section 4 introduces the simplified model of the HES, explains why it is necessary, and compares its results with the detailed model developed with MATLAB/Simulink using the Simscape Electrical library; finally, Section 5 presents a discussion of the obtained results and recommendations for further work.

2. The Case Study

Figure 1 presents the main elements of the electric power system for the wind-powered OOGPs which is used as case study in this paper. Specifically, they are: a floating wind turbine with its associated AC/AC converter and transformer (T_1); the transmission line cable; fixed loads; a GT with its associated synchronous generator (SG) and transformer (T_2); flexible loads; and an ESS with its

associated AC/DC converter. An extensive description of this model without the ESS is provided in [10], and a summary of the system parameters required for modeling is available in Table A1.

The input for the wind turbine (WT) model is the wind speed, which is interpolated with the power curve to obtain the WT output power. The wind speed is a time series from high-resolution measurements of the Sleipner weather station in the North Sea and is based on data from MET Norway [23]. This time series is filtered before interpolation by a low-pass filter representing the inertia constant of the turbine. The power curve is based on a cut-in speed of 4 m/s, nominal speed of 12 m/s, cut-out speed of 25 m/s and is available in [24]. The WT side converter operates in maximum power point tracking, and no active power curtailment is applied to regulate the grid frequency. The grid side converter controls the DC link voltage.

To simplify the representation of fixed loads in the model, they are lumped in two single loads representing the following groups: (1) loads that have minor variation in consumption during operation, such as low-voltage motors and pumps from the process, and auxiliary services (e.g., illumination and housing of personnel); (2) loads that have large, short time variations during operation, such as medium-voltage motors responsible for pumping oil or compressing gas. Please note that for the sake of simplicity, Figure 1 shows only one fixed load representing both groups.

On the other hand, flexible loads represent large, medium-voltage motors interfaced with variable speed drives. They are different from group 2 because their active and reactive power can be controlled by the EMS to provide inertial and voltage support to the grid without affecting the process performance. In this case study, the flexible load is the water injection system, which is responsible to maintain overall and hydrostatic reservoir pressures and force the oil toward the production wells [1]. This type of load is flexible because reservoir pressures can vary within a certain range, and the time constant of the system is large (i.e., minutes) when compared to the electrical system dynamics (i.e., seconds). Hence, the EMS can actively change active and reactive power of the flexible loads during a short period without affecting the overall process performance.

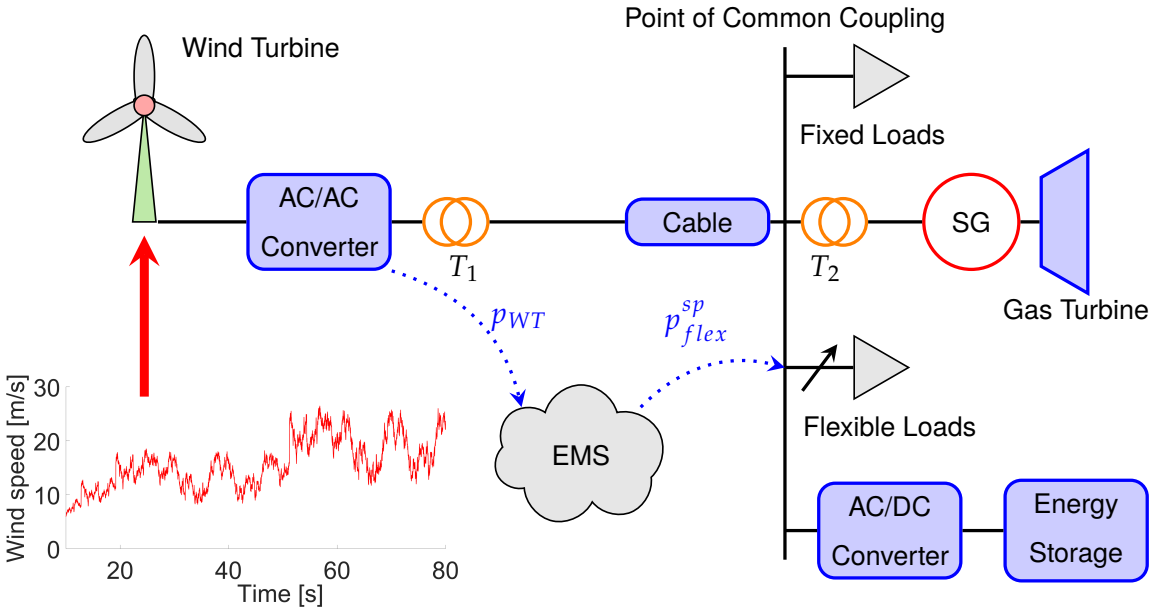

Figure 1. Main elements of the electric power system for a wind-powered OOGPs.

The smart load management proposed in [10] is also applied to this case study, i.e., the EMS dynamically adjusts the flexible load setpoint according to the WT production with a 1 s delay. In other words, if the instantaneous WT power output is 0.4 pu of the WT rated value, then the EMS will set the flexible load setpoint to 0.4 pu of the flexible load rated value. If a wind gust increases the

instantaneous WT output to 0.6 pu, then the EMS will change the flexible load setpoint to 0.6 pu after 1 s. For modeling purposes, the flexible load setpoint (p_{flex}) is represented by:

$$p_{flex}^{sp} = -\left(\frac{S_{WT}^{rated}}{S_{flex}^{rated}}\right)\left(\frac{1}{T_{comm}\,s+1}\right)p_{WT} \tag{1}$$

where p_{flex}^{sp} is the flexible load active power setpoint [pu]; p_{WT} is the WT active power [pu]; S_{flex}^{rated}, S_{WT}^{rated} are the converter rated apparent power of the flexible load and the WT respectively; and T_{comm} is the time constant of a low-pass filter. The latter is an approximation of: (1) a filter to remove measurement noise; (2) the communication delay required for interaction of the WT and flexible load with the EMS through a communication link.

It is assumed the EMS can forecast the day-ahead average wind power production (p_{WT}) and average load consumption (p_{fix}, p_{flex}) with an error of a few percent of the rated load capacity during short time intervals (>15 min and <1 h). The literature provides several examples of such forecasting algorithms: [25–27]. Accordingly, tertiary control [28] is not considered in the simulations, the EMS algorithm for optimal dispatch is not executed in real time and setpoints for the GT and ESS are assumed constant during the simulations.

The remaining of this section will focus on describing the ESS model and its proposed controller.

Energy Storage System

A model identical to the wind turbine grid side and flexible load converters is adopted for the ESS AC/DC converter, i.e., a voltage source converter (VSC) connected to the grid through a L filter. More details about modeling of this converter and tuning of its internal control loops can be obtained in [29].

To simplify the ESS model and make it technology-independent, the following assumptions are made:

- the storage device provides a constant voltage to the DC link of the VSC;
- the EMS can change the setpoint of the GT to charge or discharge the ESS;
- the state of charge (SOC) is ignored, as it is assumed the EMS can maintain a minimum SOC to guarantee inertial support to the electrical grid.

The control for the ESS is designed to provide frequency and voltage support to the electrical grid, also referred as primary control [28]. Taking this into consideration, Equations (2) and (3) present the proposed closed-loop transfer functions in the Laplace domain for the external controller of the ESS:

$$I_{dref}(s) = -\left(\frac{1}{T_{flp}\,s+1}\right)\left[\left(\frac{T_{fr}\,s}{T_{fr}\,s+1}\right)K_{ft}+\frac{K_{fi}}{s}\right]\Delta F_{PCC}(s) \tag{2}$$

$$I_{qref}(s) = -\left(\frac{1}{T_{ulp}\,s+1}\right)\left[\left(\frac{T_{ur}\,s}{T_{ur}\,s+1}\right)K_{ut}+\frac{K_{ui}}{s}\right]\Delta U_{PCC}(s) \tag{3}$$

where I_{dref} is the VSC reference current in the d-axis [pu], ΔF_{PCC} is the point of common coupling (PCC) frequency deviation from its reference value [pu], T_{flp} is the time constant of the frequency low-pass filter [s], T_{fr} is the reset time of the frequency wash-out filter [s], K_{ft} is the transient frequency droop [pu·s/pu], K_{fi} is the integral gain of the frequency controller [pu/(pu·s)], I_{qref} is the converter reference current in the q-axis [pu], ΔU_{PCC} is the PCC voltage deviation from its reference value [pu], T_{ulp} is the time constant of the voltage low-pass filter [s], T_{ur} is the reset time of the voltage wash-out filter [s], K_{ut} is the voltage transient droop [pu·s/pu], and K_{ui} is the integral gain of the voltage controller [pu/(pu·s)]. PCC frequency and voltage references are assumed as 1 pu.

The low-pass and wash-out filters combined are equivalent to a band-pass filter that eliminates the DC and high-frequency/noise values from measurements. Its frequency response can be seen in

Figure 2. Their effect together with the gain K_t is momentarily increasing the system damping when a transient occurs, hence the name transient droop. Furthermore, the integral action of the controller takes care of bringing frequency and voltage to their rated values.

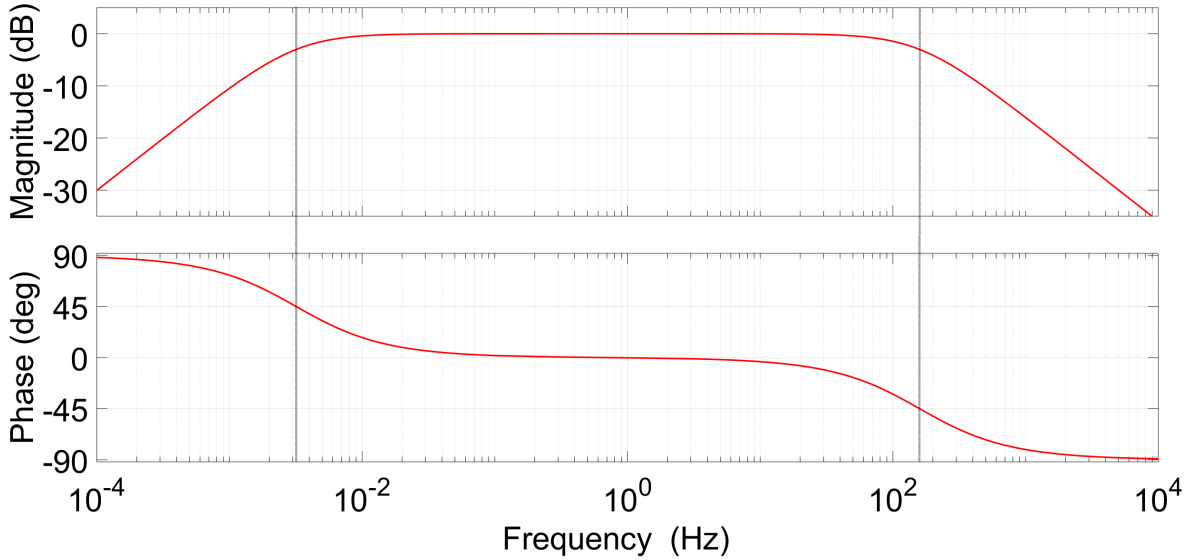

Figure 2. Frequency response of the low-pass filter combined with the wash-out filter when $K_t = 1$, $T_{lp} = 0.001$ s, $T_r = 50$ s. This combination is equivalent to a band-pass filter.

When implementing these control laws, it is important to consider some non-linearities. First, the control signal output must be limited to the rated values of the equipment. Second, whenever this occurs, an anti-windup logic must be activated in the integral part of the controller ([30] sec 9.3.1). Figure 3 presents a complete block diagram of the controller considering these non-linear effects.

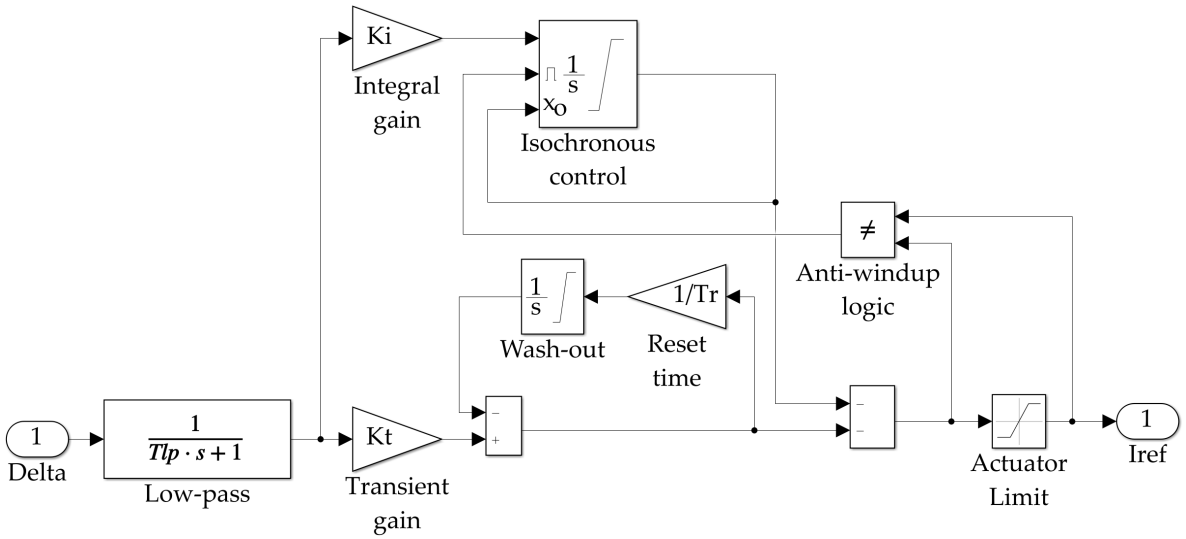

Figure 3. Block diagram of the proposed controller considering non-linear effects.

While transient droop is not a new topic in power system stability and has been explored for decades [31], the use of an ESS interfaced by a VSC provides the bandwidth required to effectively implement it. The following section provides results corroborating this affirmation.

3. Simulation Results

The purpose of this section is to demonstrate that power quality can be improved with the smart load management combined with the proposed ESS controller. For that, the system is simulated in MATLAB/Simulink with and without the ESS for a period of 80 s. Fixed loads are represented as constant impedances and flexible loads as constant power loads. The wind turbine is started at t = 10 s and two transients are considered: the largest motor in fixed load group 2 (10 MW, 0.4 pu) is switched on at t = 30 s, and then switched off at t = 65 s.

To evaluate the simulation results, some metrics are introduced:

$$f_{RMSE} = \sqrt{\frac{\sum_{n=1}^{N}(f-1)^2}{N}} \tag{4}$$

$$u_{RMSE} = \sqrt{\frac{\sum_{n=1}^{N}(u-1)^2}{N}} \tag{5}$$

$$u/f_{RMSE} = \sqrt{\frac{\sum_{n=1}^{N}(\frac{u}{f}-1)^2}{N}} \tag{6}$$

$$p_{RMSE} = \sqrt{\frac{\sum_{n=1}^{N}(p_m-p_e)^2}{N}} \tag{7}$$

where N is the number of samples for the entire simulation, f, u are respectively the PCC instantaneous frequency and voltage, p_m, p_e are respectively the instantaneous mechanical and electrical power of the GT. In summary, the proposed metrics compare the measured variables to their setpoints and do not account for the error sign. The root mean square error (RMSE) compares the accuracy of models [32] and its values vary between $\pm\infty$ (bad fit) and 0 (perfect fit).

Figure 4 presents an overview of the simulation results, while Figures 5 and 6 present details of the transients and Table 1, the metrics. For the PCC frequency, voltage and u/f curves, the area highlighted in green is the range allowed for continuous operation by typical industry standards [18,33–35]. The regions outside this area are allowed for transient operation. The domain where protection schemes are usually activated [36,37] lies beyond the y-axis limits.

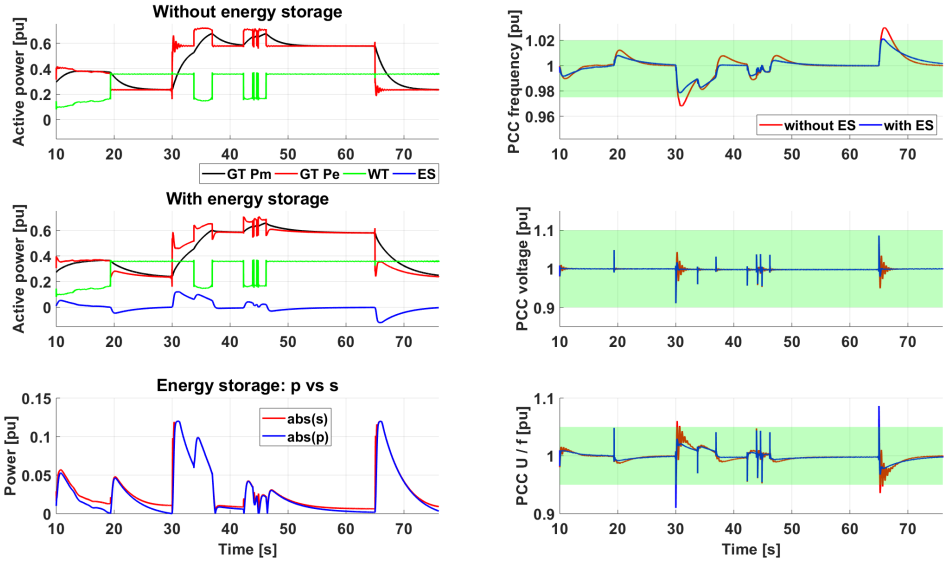

Figure 4. Active power, ESS active (p) versus apparent (s) power, PCC frequency and voltage for 10 < t < 76 s.

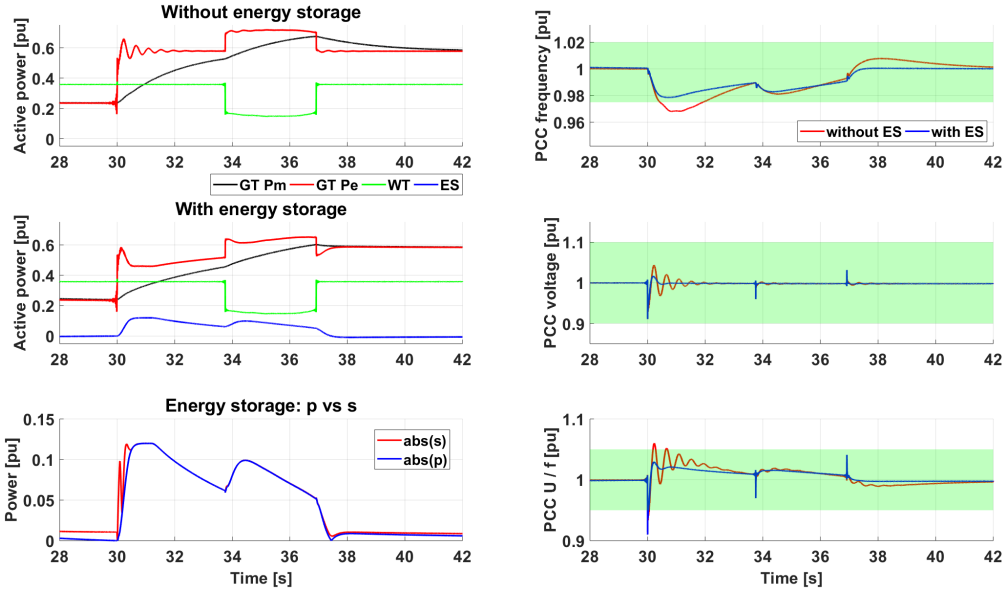

Figure 5. Detail of the period where a 10 MW load is switched on.

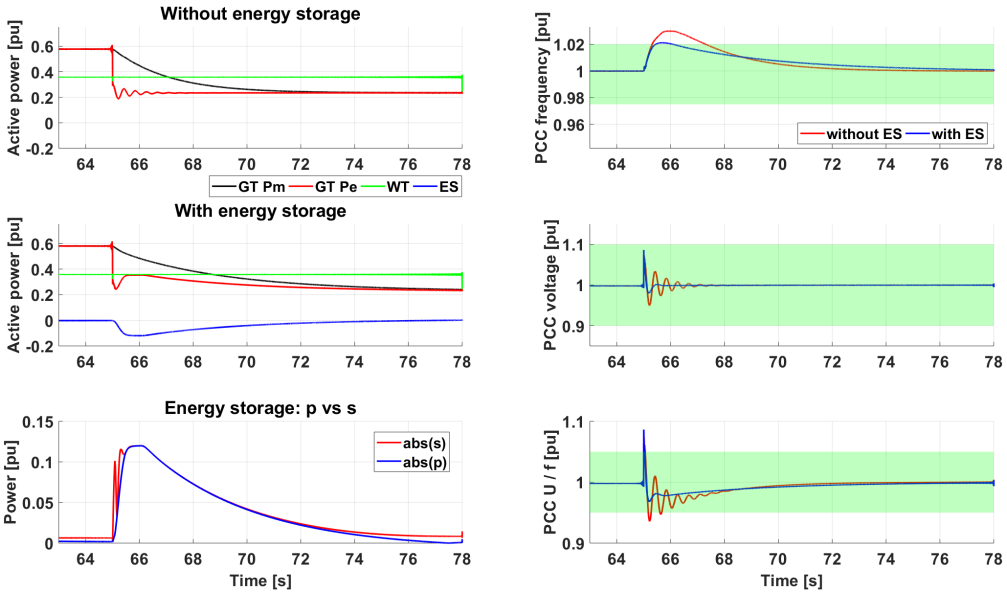

Figure 6. Detail of the period where a 10 MW load is switched off.

Table 1. Metrics obtained from the detailed model simulation results.

Metric	Without ESS	With ESS	Difference
f_{max}	1.030 pu	1.021 pu	−0.9%
f_{min}	0.968 pu	0.979 pu	1.1%
f_{RMSE}	0.009 pu	0.007 pu	−23.1%
u_{max}	1.086 pu	1.086 pu	0%
u_{min}	0.910 pu	0.910 pu	0%
u_{RMSE}	0.005 pu	0.003 pu	−37.6%
u/f_{max}	1.086 pu	1.086 pu	0%
u/f_{min}	0.910 pu	0.910 pu	0%
u/f_{RMSE}	0.010 pu	0.007 pu	−26.9%
p_{RMSE}	0.071 pu	0.056 pu	−21.8%
$\frac{p_{mGT}}{dt}max$	0.130 pu/s	0.096 pu/s	−26.2%

Some interesting observations from the simulation results are:

- When analyzing f_{max}, f_{min} values, one will notice that the proposed controller is not able to substantially improve these indicators. This can be justified by the fact that the ESS has a relatively small power capacity (0.18 pu) when compared to the rated power of the WT (0.36 pu) and GT (1 pu);
- When considering f_{RMSE} values, the proposed controller reduces frequency deviations considerably (−23.1%). This is visually confirmed in Figure 4 when comparing the amount of time outside the continuous operation range in both cases;
- When analyzing $u_{max}, u_{min}, u/f_{max}, u/f_{min}$ values, one will notice that the proposed controller is not able at all to improve these indicators. This is justified by the fact that the controller bandwidth is not large enough to counteract the voltage spikes induced by abrupt power flow changes;
- When referring to u_{RMSE} values, the proposed controller reduces voltage oscillations dramatically (−37.6%). This is visually confirmed in Figures 5 and 6 when comparing the required time for damping oscillations in both cases.
- Improvements in u_{RMSE}, f_{RMSE} with the ESS are also reflected in u/f_{RMSE};
- Figures 5 and 6 indicate that the damping of voltage oscillations has also a positive effect on the reduction of active power oscillations. This confirms the controller efficacy in voltage support and suggests that such control scheme also provides a power system stabilizer functionality;
- For the case without ESS, the peak rate of change of the GT mechanical power $\frac{dp_{mGT}}{dt}max$ is very close to the maximum allowed value for a typical GT used in OOGP (e.g., 0.15 pu/s for GE LM2500 [38]). This is greatly alleviated with the ESS (−26.2%), which confirms the controller efficacy in transient inertial support;
- For the case with ESS, the ESS energy throughput is 4.96 kWh during the 10 MW load switch on (with wind variations), and 4.17 kWh during the 10 MW load switch off (no wind variations). It is interesting to notice that wind variability affects considerably (+18.9%) the energy throughput during a disturbance;
- The difference between absolute values of the ESS active (p) and apparent (s) power are minimal (RMSE = 0.0065 pu).

4. Simplified Model

For assessment and early design purposes, the impact of a given ESS in an HES should be easy and fast to evaluate. In particular, given a specific ESS configuration and the forecast of renewable sources (e.g., wind speed, solar irradiance, sea state) and load consumption, it should be straight to obtain the expected power production of all generators, and the ESS peak apparent power, power flow and energy throughput. Those are key input variables for the state-of-the-art optimization procedures tackling the ESS sizing problem [13–17]. As described earlier in Section 1, a common simplification in those optimization procedures is assuming steady-state equations to obtain the active power balance in the system. This means that PCC frequency variations and power quality requirements are currently ignored.

On one hand, an ESS can play a significant role in improving power quality, as shown in Section 3. On the other hand, the model developed in Section 2 is very detailed, and many of its parameter values are not available during the assessment and early design phases of an HES. Not least, its total execution time on standard office computers can make its application impractical in current optimization algorithms, which are based on the evaluation of thousands of different scenarios.

Keeping this context in mind, the authors derives a simplified model for the HES using a procedure similar to those outlined in [39]. The frequency dynamics are evaluated using the equations of motion from a SG ([40] ch.5):

$$\frac{2H}{\omega_m}\frac{d\omega_m}{dt} = \Delta p \tag{8}$$

$$\Delta p = p_m - p_e - p_d \tag{9}$$

$$p_d = \omega_m k_d \Delta\omega_m \tag{10}$$

$$\Delta\omega_m = \omega_{mref} - \omega_m \tag{11}$$

where H is the equivalent inertia constant of the system [s], ω_m is the equivalent mechanical angular speed [pu], Δp is the instantaneous accelerating power [pu], p_m, p_e, p_d are respectively the equivalent mechanical power [pu], electrical power [pu] and power provided by the damper windings [pu], k_d is the damping constant [pu/pu], ω_{mref} is the reference or rated angular speed [pu], assumed as 1 pu for all simulations. Figure 7 presents a block diagram of this subsystem.

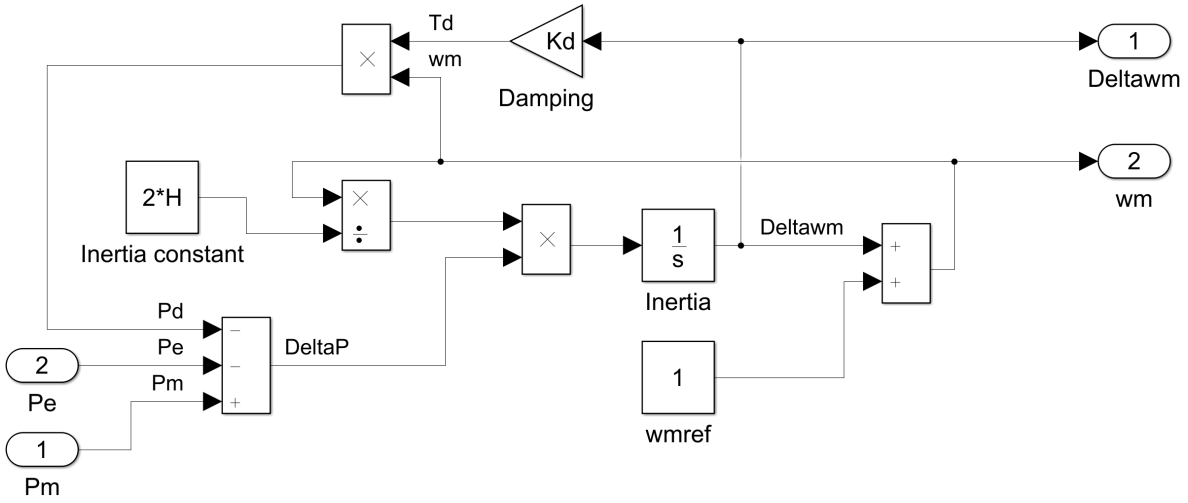

Figure 7. Simplified model of the HES as a SG.

The voltage dynamics are not evaluated in the simplified model because they have negligible impact on the ESS sizing problem. When analyzing the voltage regulation law (Equation (3)), one will notice that it influences I_q of the VSC and, as so, the reactive power of the ESS. As seen in Section 3, the contribution of reactive power to the apparent power of the VSC is negligible. Hence, it is assumed the ESS active power is a good approximation of its apparent power.

In the simplified model, the same frequency controllers from the detailed model are used, i.e., the simplified GT governor [40] and the proposed ESS VSC external controller (Equation (2)). The ESS VSC behavior is approximated by a first-order low-pass filter.

Finally, to complete the model, the electrical power is assumed as:

$$p_e = p_{flex} + p_{fix} - p_{WT} - p_{ES} \tag{12}$$

where p_{flex}, p_{fix} are respectively the power demanded by the flexible and fixed loads [pu], and p_{WT}, p_{ES} are respectively the power supplied by the WT and the ESS [pu].

4.1. Model Validation

The purpose of this section is to validate the proposed simplified model against the detailed model developed with MATLAB/Simulink presented in Section 2. For that, the simplified model is simulated under the same conditions as previously described in Section 3. Figures 8 and 9 show a comparison of the simplified and detailed models in two scenarios, i.e., with and without the ESS. Moreover, Table 2

compares the goodness of fit between the two models using minimum and maximum values, as well as the normalized mean square error (NMSE), defined as:

$$NMSE = 1 - \frac{\|x_{ref} - x\|^2}{\|x_{ref} - \bar{x}_{ref}\|^2} \tag{13}$$

where $\|$ indicates the Euclidean or L^2 norm of a vector, and the reference is the detailed model. The NMSE is an estimator of the overall deviations between a reference model (x_{ref}) and the measured values (x), and its values vary between $-\infty$ (bad fit) to 1 (perfect fit) [32].

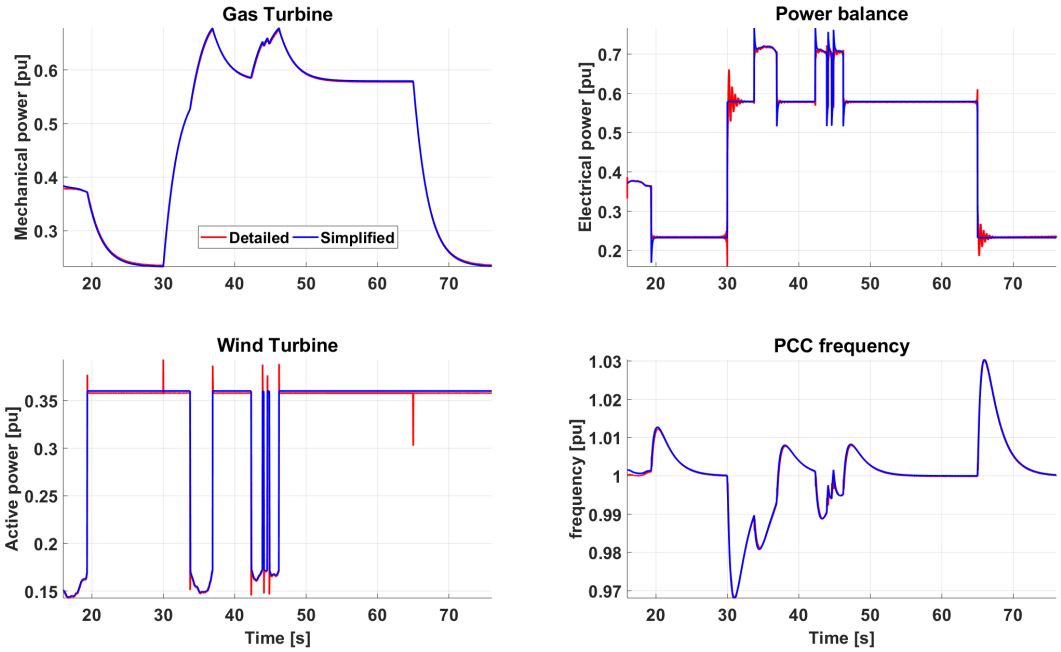

Figure 8. Detailed versus simplified model without ESS.

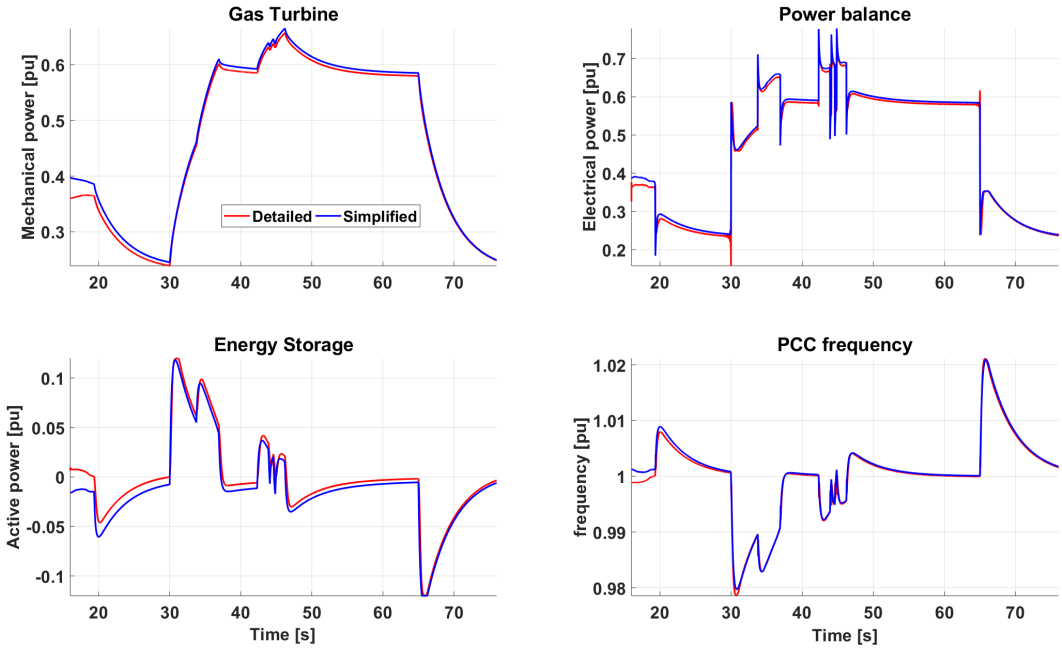

Figure 9. Detailed versus simplified model with ESS.

Table 2. Metrics comparing the detailed and simplified models.

Metric	Without ESS		With ESS	
	[pu]	[%]	[pu]	[%]
Δp_{GTmax}	0.003	0.4	0.008	1.2
Δp_{GTmin}	−0.002	−0.8	0.006	2.7
p_{GTNMSE}	0.999	-	0.996	-
Δp_{emax}	0.044	6.1	0.071	10.0
Δp_{emin}	0.009	6.00	0.026	16.7
p_{eNMSE}	0.997	-	0.995	-
Δp_{WTmax}	−0.017	−4.4	−0.017	−4.4
Δp_{WTmin}	0.014	10.8	0.014	10.8
p_{WTNMSE}	0.998	-	0.998	
Δp_{ESmax}	-	-	−0.002	−1.3
Δp_{ESmin}	-	-	0.000	0
p_{ESNMSE}	-	-	0.955	-
Δf_{max}	0.001	0.1	0.000	0
Δf_{min}	0.000	0	0.001	0.1
f_{NMSE}	0.998	-	0.993	

Some relevant observations emerge from the comparison:

- For both scenarios, some steady-state errors are observed. This is clearly seen in Figure 8 in the offset of the p_{WT}, and in Figure 9 in the offset of the p_{ES} curves. Those also affect p_e, p_{GT}, as they are correlated by Equation (12). This is expected, as the simplified model considers only power flows and ignores ohmic losses;
- The simplified model approximates frequency dynamics really well for both scenarios, as seen by the negligible values of $\Delta f_{max}, \Delta f_{min}$, as well as f_{NMSE} very close to 1;
- The simplified model gives considerable absolute errors in both scenarios for variables that are influenced by the voltage dynamics, namely p_e, p_{WT}. This is seen on the metrics $\Delta p_{emax}, \Delta p_{emin}, \Delta p_{WTmax}, \Delta p_{WTmin}$. This is expected, as the simplified model ignores voltage dynamics, hence voltage spikes and power oscillations are not captured. However, p_{eNMSE}, p_{WTNMSE} are close to 1, which shows that the goodness of fit of the simplified model for those variables is accurate;
- The GT mechanical power and ESS active power are very well captured by the simplified model. Absolute errors present small values, i.e., $\Delta p_{GTmax}, \Delta p_{GTmin}, \Delta p_{ESmax}, \Delta p_{ESmin}$. On the other hand, while p_{GTNMSE} gives an almost perfect goodness of fit, p_{ESNMSE} is penalized by the steady-state error;
- For the scenario with ESS, the ESS energy throughput is 4.51 kWh during the 10 MW load switch on, and 4.53 kWh during the 10 MW load switch off. This represents respectively errors of −9.1% and +8.6% when compared to the detailed model. The reason for those large deviations is the steady-state error between p_{ES} in both models;
- The required simulation steps are 20 µs for the detailed model and 1ms for the simplified model. Moreover, the latter has no VSCs and their associated control loops, what reduces dramatically the model complexity and total simulation time. For reference purposes, the detailed and simplified model run respectively in 694 and 1.1 s in a laptop equipped with MATLAB 2018a, an Intel Core i7-8650U CPU at 2.11 GHz, and 16 GB of RAM.

5. Discussion and Further Work

As seen in Section 3, an ESS with the proposed controllers effectively contributes to increase power quality in the HES studied. For a wind-powered OOGP in islanded mode, this brings some advantages.

Firstly, the ESS may help to reduce the negative impact of intermittent energy sources on the maintenance and reliability of other equipment. Reduced frequency deviations translate into less

actuation of the GT governor and thus less wear and tear of electromechanical actuators. Furthermore, the ESS provides inertial support that reduces the peak rate of change of the GT power. The latter may not only contribute to less mechanical stresses but also to the reduction of GHG emissions. Finally, the voltage support provided by the ESS damps active power oscillations. This in turn reduces torque pulsations not only at the shaft of the GT, but also in motors connected to the grid without a motor drive.

Secondly, the additional inertial support provided by the ESS may allow the operation of only one GT in a wind-powered OOGP meeting the power quality limits required by industry standards. This opens the possibility to review redundant hot-standby schemes of GTs that are typical in traditional OOGP, by either operating the second GT in cold-standby or even eliminating it at all. This allows operation of the active GT in better efficiency points, and consequently a reduction of GHG emissions, especially if combined with waste heat recovery units.

In this context, topics to be further developed are a more detailed investigation about reliability and maintenance issues of GT and motors affected by intermittent energy sources in HES, and the best control strategies to reduce GHG in a HES.

However, the operation of the ESS providing inertial support requires additional energy throughput that is proportional to the frequency variations in the HES. Therefore, an efficient simplified model that can estimate frequency variations with accuracy is necessary to provide key input variables for optimization procedures tackling the ESS sizing and economical dispatch problems. Section 4 provides a procedure to derive such model for the OOGP case study described in Section 2. It is worth emphasizing that the methods presented can be easily extended to other types of HES, despite the focus on the OOGP application.

The results presented in Section 4.1 suggest that the proposed simplified model serves its purpose, i.e., it captures the frequency dynamics of the HES with a high level of accuracy when compared to a detailed model developed with Matlab/Simulink using the Simscape Electrical library. It also provides estimations of the ESS peak power and energy throughput that are accurate enough for design purposes, with a total simulation time at least two orders of magnitude lower than the detailed model. This allows the proposed model to be incorporated in optimization algorithms evaluating a huge number of scenarios.

Hence, a natural step further in future research may be to incorporate new constraints based on power quality requirements in the state-of-the-art ESS sizing procedures. This may also involve the optimization of the ESS sizing based on constraints such as apparent power peak rate of change, and the application of distinct storage technologies for different needs.

Nevertheless, the proposed simplified model has also drawbacks. First, it does not capture voltage dynamics and power oscillations of the electrical grid. While these may not be so critical in an OOGP, they will certainly be relevant to evaluate the stability of a hybrid energy system connected to distribution grids with high impedance and limited power transfer capacity. Moreover, steady-state errors of the proposed model generate significant errors in the estimated energy throughput of the ESS. Therefore, the ability of this model to provide a reliable SOC estimation may be compromised, especially for very long periods.

Author Contributions: Conceptualization, E.A. and E.T.; methodology, E.A. and S.S.; software, E.A. and S.S.; validation, E.A.; formal analysis, E.A.; investigation, E.A.; resources, S.S., D.B. and E.T.; data curation, E.A.; writing—original draft preparation, E.A.; writing—review and editing, S.S., D.B. and E.T.; visualization, E.A.; supervision, D.B. and E.T.; project administration, E.T.; funding acquisition, E.T.

Funding: This research was funded by the Research Council of Norway under the program PETROMAKS2, grant number 281986, project "Innovative Hybrid Energy System for Stable Power and Heat Supply in Offshore Oil & Gas Installation (HES-OFF)".

Acknowledgments: Danilo Brandao and Elisabetta Tedeschi were supported by the Research Council of Norway under the grant number 261735, project "Norwegian-Brazilian collaboration on Power Theories and Cooperative Control for Renewable Energy Integration (NB_POCCREI)".

Conflicts of Interest: The authors declare no conflict of interest.

Abbreviations

The following abbreviations are used in this manuscript:

EMS	energy management system
ESS	energy storage system
GHG	greenhouse gas
GT	gas turbine
HES	hybrid energy system
NMSE	normalized mean square error
OOGP	offshore oil and gas platform
PCC	point of common coupling
RMSE	root mean square error
SG	synchronous generator
SOC	state of charge
VSC	voltage source converter
WT	wind turbine

Appendix A

Table A1. Summary of the model parameters for the case study.

Parameter	Value	Unit	Parameter	Value	Unit
Base values			*Simulink configurations*		
Apparent power	25	MVA	Simulink solver	Fixed-step ode4	-
Line voltage	11	kV	powergui discrete solver	TBE	-
Frequency	50	Hz			
SG			*Exciter*		
Apparent power	1	pu	IEEE421.5 [41] Type	AC1C	-
Number of poles	2	pairs	Ka	20	pu/pu
Shunt resistance	0.002	pu	Ke	0.8	pu/pu
Shunt reactance	0.3	pu	Kf	0.01	pu/pu
Inertia constant	1.85	s	Ta	0.02	s
Damping factor	7.04	pu/pu	Tb	0.2	s
			Tc	1.2	s
			Te	0.5	s
			Tf	0.35	s
Turbine governor			*Fixed loads rated power*		
Permanent droop	0.8222	pu/pu	Load 1	(0.4727 + j0.0834)	pu
Actuator delay	2.25	s	Load 2	(0.3464 + j0.2000)	pu
Wind speed			*Flexible load setpoint*		
Low-pass filter time constant	1.2	s	Low-pass filter time constant	1	s
WT VSC			*ESS and flexible load VSCs*		
Apparent power	0.36	pu	Apparent power	0.18	pu
Filter inductance	12.6	mH	Filter inductance	25.2	mH
Filter shunt resistance	121	mΩ	Filter shunt resistance	242	mΩ
Filter capacitance	4	μF			
Filter parallel resistance	13.2	Ω			
dq current proportional gain	0.5556	pu/pu	dq current proportional gain	0.5556	pu/pu
dq current integral gain	5.3333	pu/s	dq current integral gain	5.3333	pu/s

Table A1. *Cont.*

Parameter	Value	Unit	Parameter	Value	Unit
ESS frequency controller			*ESS voltage controller*		
Transient droop	50	pu/pu	Transient droop	20	pu/pu
Transient reset time	50	s	Transient reset time	50	pu/pu
Low-pass filter time	0.001	s	Low-pass filter time	0.001	s
Integral gain	0.2	s	Integral gain	0.2	pu/s

References

1. Devold, H. *Oil and Gas Production Handbook: An Introduction to Oil and Gas Production*; OCLC: 1058182209; Lulu. com.: Morrisville, NC, USA, 2013.
2. Bothner, T.M.; Høie, H. *Utslipp av Klimagasser*; Technical Report; Statistik Sentralbyrå: Oslo, Norway, 2018.
3. Korpås, M.; Warland, L.; He, W.; Tande, J.O.G. A Case-Study on Offshore Wind Power Supply to Oil and Gas Rigs. *Energy Procedia* **2012**, *24*, 18–26. [CrossRef]
4. He, W.; Uhlen, K.; Hadiya, M.; Chen, Z.; Shi, G.; del Rio, E. Case Study of Integrating an Offshore Wind Farm with Offshore Oil and Gas Platforms and with an Onshore Electrical Grid. *J. Renew. Energy* **2013**, *2013*, 607165. [CrossRef]
5. Kolstad, M.L.; Årdal, A.R.; Sharifabadi, K.; Undeland, T.M. Integrating Offshore Wind Power and Multiple Oil and Gas Platforms to the Onshore Power Grid Using VSC-HVDC Technology. *Mar. Technol. Soc. J.* **2014**, *48*, 31–44. [CrossRef]
6. Riboldi, L.; Nord, L.O. Concepts for Lifetime Efficient Supply of Power and Heat to Offshore Installations in the North Sea. *Energy Convers. Manag.* **2017**, *148*, 860–875. [CrossRef]
7. Legorburu, I.; Johnson, K.R.; Kerr, S.A. Multi-Use Maritime Platforms—North Sea Oil and Offshore Wind: Opportunity and Risk. *Ocean Coast. Manag.* **2018**, *160*, 75–85. [CrossRef]
8. Isaksen, E.A. Wind Farm Being Considered at Snorre and Gullfaks. Available online: https://www.equinor.com/en/news/27aug2018-hywind-tampen.html (accessed on 29 July 2019).
9. Marvik, J.I.; Øyslebø, E.V.; Korpås, M. Electrification of Offshore Petroleum Installations with Offshore Wind Integration. *Renew. Energy* **2013**, *50*, 558–564. [CrossRef]
10. Sanchez, S.; Tedeschi, E.; Silva, J.; Jafar, M.; Marichalar, A. Smart Load Management of Water Injection Systems in Offshore Oil and Gas Platforms Integrating Wind Power. *IET Renew. Power Gener.* **2017**, *11*, 1153–1162. [CrossRef]
11. *IEEE Std 1547.4-2011: IEEE Guide for Design, Operation, and Integration of Distributed Resource Island Systems with Electric Power Systems*; OCLC: 762137491; IEEE: New York, NY, USA, 2011.
12. *IEEE Std 2030.2-2015: IEEE Guide for the Interoperability of Energy Storage Systems Integrated with the Electric Power Infrastructure*; OCLC: 923758286; IEEE: New York, NY, USA, 2015.
13. Chen, S.X.; Gooi, H.B.; Wang, M.Q. Sizing of Energy Storage for Microgrids. *IEEE Trans. Smart Grid* **2012**, *3*, 142–151. [CrossRef]
14. Bahramirad, S.; Reder, W.; Khodaei, A. Reliability-Constrained Optimal Sizing of Energy Storage System in a Microgrid. *IEEE Trans. Smart Grid* **2012**, *3*, 2056–2062. [CrossRef]
15. Dong, J.; Gao, F.; Guan, X.; Zhai, Q.; Wu, J. Storage-Reserve Sizing With Qualified Reliability for Connected High Renewable Penetration Micro-Grid. *IEEE Trans. Sustain. Energy* **2016**, *7*, 732–743. [CrossRef]
16. Fossati, J.P.; Galarza, A.; Martín-Villate, A.; Fontán, L. A Method for Optimal Sizing Energy Storage Systems for Microgrids. *Renew. Energy* **2015**, *77*, 539–549. [CrossRef]
17. Wong, L.A.; Ramachandaramurthy, V.K.; Taylor, P.; Ekanayake, J.; Walker, S.L.; Padmanaban, S. Review on the Optimal Placement, Sizing and Control of an Energy Storage System in the Distribution Network. *J. Energy Storage* **2019**, *21*, 489–504. [CrossRef]
18. *IEEE Std 1547-2018: IEEE Standard for Interconnection and Interoperability of Distributed Energy Resources with Associated Electric Power Systems Interfaces*; OCLC: 1048178696; IEEE: New York, NY, USA, 2018.
19. Aghamohammadi, M.R.; Abdolahinia, H. A New Approach for Optimal Sizing of Battery Energy Storage System for Primary Frequency Control of Islanded Microgrid. *Int. J. Electr. Power Energy Syst.* **2014**, *54*, 325–333. [CrossRef]

20. Ulleberg, Ø. The Importance of Control Strategies in PV–Hydrogen Systems. *Sol. Energy* **2004**, *76*, 323–329. [CrossRef]
21. Dufo-López, R.; Bernal-Agustín, J.L.; Contreras, J. Optimization of Control Strategies for Stand-Alone Renewable Energy Systems with Hydrogen Storage. *Renew. Energy* **2007**, *32*, 1102–1126. [CrossRef]
22. Bernal-Agustín, J.L.; Dufo-López, R. Simulation and Optimization of Stand-Alone Hybrid Renewable Energy Systems. *Renew. Sustain. Energy Rev.* **2009**, *13*, 2111–2118. [CrossRef]
23. MET Norway. Frost API. Available online: https://frost.met.no/index.html (accessed on 29 July 2019).
24. Nielsen, F.G. Hywind—From Idea to World's First Wind Farm Based upon Floaters. Available online: https://www.uib.no/sites/w3.uib.no/files/attachments/hywind_energy_lab.pdf (accessed on 29 July 2019).
25. Pappala, V.; Erlich, I.; Rohrig, K.; Dobschinski, J. A Stochastic Model for the Optimal Operation of a Wind-Thermal Power System. *IEEE Trans. Power Syst.* **2009**, *24*, 940–950. [CrossRef]
26. Kuznetsova, E.; Li, Y.F.; Ruiz, C.; Zio, E. An Integrated Framework of Agent-Based Modelling and Robust Optimization for Microgrid Energy Management. *Appl. Energy* **2014**, *129*, 70–88. [CrossRef]
27. Chapaloglou, S.; Nesiadis, A.; Iliadis, P.; Atsonios, K.; Nikolopoulos, N.; Grammelis, P.; Yiakopoulos, C.; Antoniadis, I.; Kakaras, E. Smart Energy Management Algorithm for Load Smoothing and Peak Shaving Based on Load Forecasting of an Island's Power System. *Appl. Energy* **2019**, *238*, 627–642. [CrossRef]
28. Guerrero, J.M.; Vasquez, J.C.; Matas, J.; de Vicuna, L.G.; Castilla, M. Hierarchical Control of Droop-Controlled AC and DC Microgrids—A General Approach Toward Standardization. *IEEE Trans. Ind. Electron.* **2011**, *58*, 158–172. [CrossRef]
29. Suul, J.A.; Molinas, M.; Norum, L.; Undeland, T. Tuning of Control Loops for Grid Connected Voltage Source Converters. In Proceedings of the 2008 IEEE 2nd International Power and Energy Conference, Johor Bahru, Malaysia, 1–3 December 2008; IEEE: Piscataway, NJ, USA, 2008; pp. 797–802. [CrossRef]
30. Franklin, G.F.; Powell, J.D.; Emami-Naeini, A. *Feedback Control of Dynamic Systems*, 6th ed.; OCLC: 845656750; Pearson: Upper Saddle River, NJ, USA, 2010.
31. Patel, R.; Bhatti, T.S.; Kothari, D.P. Improvement of Power System Transient Stability Using Fast Valving: A Review. *Electr. Power Components Syst.* **2001**, *29*, 927–938. [CrossRef]
32. Lewis-Beck, C.; Lewis-Beck, M. *Applied Regression: An Introduction*; SAGE Publications, Inc.: Thousand Oaks, CA, USA, 2016.[CrossRef]
33. *NORSOK E-001:2016 Electrical Systems*, 6th ed.; NTS: Oslo, Norway, 2016.
34. *IEC 61892:2015 Mobile and Fixed Offshore Units—Electrical Installations*, 3rd ed.; IEC: Geneva, Switzerland, 2015.
35. *IEEE Std C50.13-2014: IEEE Standard for Cylindrical-Rotor 50 Hz and 60 Hz Synchronous Generators Rated 10 MVA and Above*; OCLC: 1096667824; IEEE: Piscataway, NJ, USA, 2014.
36. *IEEE Std C37.102: IEEE Guide for AC Generator Protection*; IEEE: New York, NY, USA, 2006. [CrossRef]
37. *IEEE Std C37.106: IEEE Guide for Abnormal Frequency Protection for Power Generating Plants*; IEEE: New York, NY, USA, 2004. [CrossRef]
38. Badeer, G.H. GE Aeroderivative Gas Turbines-Design and Operating Features; GE Power Systems: Evendale, OH, USA, 2000.
39. Mahmoud, M.; Azher Hussain, S.; Abido, M. Modeling and Control of Microgrid: An Overview. *J. Frankl. Inst.* **2014**, *351*, 2822–2859. [CrossRef]
40. Machowski, J.; Bialek, J.W.; Bumby, J.R. *Power System Dynamics: Stability and Control*, 2nd ed.; OCLC: Ocn232130756; Wiley: Chichester, UK, 2008.
41. *IEEE Std 421.5-2016: IEEE Recommended Practice for Excitation System Models for Power System Stability Studies*, 2016th ed.; IEEE: New York, NY, USA, 2016.